

A 3D model with shape prior information for biological structures reconstruction using Multiple-Angle Total Internal Reflection Fluorescence Microscopy

Emmanuel Soubies, Laure Blanc-Féraud, Sébastien Schaub, Gilles Aubert

► **To cite this version:**

Emmanuel Soubies, Laure Blanc-Féraud, Sébastien Schaub, Gilles Aubert. A 3D model with shape prior information for biological structures reconstruction using Multiple-Angle Total Internal Reflection Fluorescence Microscopy. ISBI - International Symposium on Biomedical Imaging, Apr 2014, Beijing, China. pp.608 - 611, 10.1109/ISBI.2014.6867944 . hal-00914998

HAL Id: hal-00914998

<https://hal.inria.fr/hal-00914998>

Submitted on 6 Dec 2013

HAL is a multi-disciplinary open access archive for the deposit and dissemination of scientific research documents, whether they are published or not. The documents may come from teaching and research institutions in France or abroad, or from public or private research centers.

L'archive ouverte pluridisciplinaire **HAL**, est destinée au dépôt et à la diffusion de documents scientifiques de niveau recherche, publiés ou non, émanant des établissements d'enseignement et de recherche français ou étrangers, des laboratoires publics ou privés.

A 3D MODEL WITH SHAPE PRIOR INFORMATION FOR BIOLOGICAL STRUCTURES RECONSTRUCTION USING MULTIPLE-ANGLE TOTAL INTERNAL REFLECTION FLUORESCENCE MICROSCOPY.

Emmanuel Soubies¹, Laure Blanc-Féraud¹, Sébastien Schaub² and Gilles Aubert³

¹ Université Nice Sophia Antipolis, I3S, CNRS, Sophia Antipolis, France.

² Université Nice Sophia Antipolis, iBV, CNRS, INSERM, Nice, France.

³ Université Nice Sophia Antipolis, Laboratoire J.A. Dieudonné, CNRS, Nice, France.

ABSTRACT

We propose a new model for the reconstruction of biological structures using Multiple-Angle Total Internal Reflection Fluorescence Microscopy (MA-TIRFM). This recent microscopy technique allows the visualization of sub-cellular structures around the plasma membrane which is of fundamental importance in the comprehension of exchanges mechanisms of the cell. We present a 3D reconstruction method based on a shape prior information on the observed structures and robust to shot noise and background fluorescence. A novelty with respect to the state of the art is to propose a method allowing the recovery of multiple objects aligned along the axial axis. The optimization problem can be formulated as a minimization problem where both the number of objects in the model and their parameters have to be estimated. This difficult combinatorial optimization problem is tackled by using a Marked Point Process approach which allows modelling interactions between the objects in order to regularize the inverse problem. Finally, performances of the proposed method are evaluated on synthetic data and real data.

Index Terms— 3D reconstruction, Total Internal Reflection Fluorescence Microscopy, Vesicles reconstruction, Evanescent wave microscopy

1. INTRODUCTION

Current researches in biology require the visualisation of finer and finer structures in order to understand tumor organisation and development. Such three-dimensional structures can be observed by fluorescence microscopy techniques; however, the axial resolution of these instruments, because of the limitations of conventional optics, is restricted to a few hundred of nanometers (e.g. ~ 500 nm for confocal microscope).

Total Internal Reflection Fluorescence Microscopy gives access to a single layer of ~ 100 nm behind the glass coverslip ($5\times$ better, in terms of axial resolution, than confocal) and provides low background fluorescence and high signal-to-noise ratio images. While single TIRFM acquisition is a unique projection of the observed volume and can not provide 3D information, developing algorithms dedicated to Multiple-Angle TIRFM (MA-TIRFM) allows to reconstruct 3D structures and overcome the axial resolution of single TIRFM by taking TIRFM acquisitions at different incident angles.

Our aim in this work is to propose a 3D reconstruction model with shape prior information which is robust to image degradations

(i.e. shot noise and background fluorescence). Some previous works on the estimation of axial positions from MA-TIRFM have been developed. Truskey *et al.* [1] and Ölveczky *et al.* [2] were interested in estimating cell/substratum separation distance. Axial position of the membrane is estimated for each pixel using a one-dimensional geometry but ignoring membrane continuity information. Both proposed methods does not consider shot noise and background fluorescence. Position and diameter of secretory granules have been studied by Rohrbach [3] and Loerke *et al.* [4]. They deal with *isolated* granules and model them by spherical (Rohrbach) and cubic (Loerke) volumes. The proposed models ignore the Poisson noise (i.e. shot noise) due to the photon collection process. More recently, Yang *et al.* [5] proposed a 3D reconstruction method of microtubules based on a statistical framework. Axial positions along the segmented curvilinear structures are computed using a Maximum A Posteriori estimator taking into account the Poisson noise. A MAP-Bayesian method is also used by Liang *et al.* [6] for 3D particle estimation. All of these methods make the strong assumption that *at a given position (x, y) there is only one object along the axial axis*. This is a simplifying assumption. In this study, we propose a new model that does not require this assumption. The difficulty of recovering multiple objects for a given radial position (x,y) is tackled by using object modelling in the Marked Point Process (MPP) framework.

The paper is organized as follows. In section 2 we formalize the reconstruction problem. Section 3 describes the proposed model and the Marked Point Process framework used to estimate object parameters. Finally, some numerical results are presented in section 4.

2. PROBLEM STATEMENT

Total internal reflection of a light beam, at the interface between two mediums of refractive indices n_i (incident) and n_t (transmitted), occurs when the incident angle α become greater than a critical angle α_c defined by $\sin(\alpha_c) = n_t/n_i$. This phenomenon produces an evanescent wave capable of exciting fluorophores that are near the dielectric surface. Theoretically, the axial profile of the evanescent wave decreases according to the law [7]:

$$I(z, \alpha) = I_0(\alpha) \exp\left(-\frac{z}{d(\alpha, \lambda)}\right) \quad (1)$$

where $I_0(\alpha)$ is the intensity at the interface (i.e. $z = 0$), $d(\alpha, \lambda) = \lambda/(4\pi n_i)(\sin^2(\alpha) - \sin^2(\alpha_c))^{-1/2}$ is the penetration depth and λ is the incident light wavelength. Excited fluorophores emit photons that are then collected by a CCD camera.

Contact: soubies@i3s.unice.fr, laure.blanc_feraud@inria.fr, sebastien.schaub@unice.fr, gilles.aubert@unice.fr

Let $R(x, y, z)$ denote the 3D unknown fluorophore density and $\mathcal{I}_2 \subset \mathbb{R}^2$ the (continuous) 2D observed image space. TIRF image formation is formulated as follows [7]:

$$\forall (x, y) \in \mathcal{I}_2, \alpha_{crit} < \alpha < \alpha_{max},$$

$$S(x, y, \alpha) = \int_0^\infty R(x, y, z) \exp\left(-\frac{z}{d(\alpha, \lambda)}\right) dz \quad (2)$$

where $S(x, y, \alpha)$ is the recorded image for the incident angle α . The intensity I_0 (in equation (1)) is known theoretically from Fresnel formulas [7], so the observed data S can be normalized by I_0 and we can omit this term in model (2). Note that because of the thinness of the evanescent wave penetration depth, the *point spread function* (PSF) along the axial direction can be set to 1 that is why it does not appears in (2).

Figure 1 contains an example of MA-TIRFM from a sample of cortactin. It is readily seen from these images that when the penetration depth decreases (from left to right), some fluorophores are not excited anymore. These structures are the deeper ones and so we can get 3D information from this set of images. The problem is then to determine R in (2) from acquisitions S_α with different incident angles.

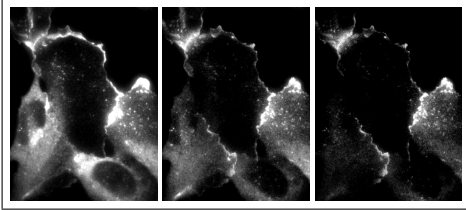


Fig. 1. Multiple-angle TIRFM (MA-TIRFM) acquisitions from a cortactin sample (protein involved in cell adhesion). Left : deeper penetration depth. Right : thinner penetration depth.

3. 3D RECONSTRUCTION METHOD

3.1. Introduction and Notations

Since problem (2) is an ill-posed inverse problem, direct inversion is not possible and a regularization is essential. The 3D unknown fluorophore density can be seen as a collection of parametrized objects and this prior information is introduced in the solution. The problem is then to determine R as a configuration of parametrized objects which satisfies equation (2).

Object modelling: Let $\mathcal{O}(\rho, \omega) \subset \mathbb{R}^3$ denotes an object defined on a state space $\mathcal{X} = P \times M$ by its location $\rho \in P$ and its marks (i.e geometric attributes $\omega \in M$)¹. Since the number of objects is unknown, we aim both at finding this number denoted $N_{\mathcal{O}} \in \mathbb{N}$ and the best sets of parameters $\{\rho_j, \omega_j\} \in \mathcal{X}$, $j \in \{1, \dots, N_{\mathcal{O}}\}$ with respect to the observed data S_{α_l} , $l \in \{1, \dots, L\}$ where L is the number of incident angles used. In the following, we denote by \mathbf{x} a configuration containing $N_{\mathcal{O}}$ objects.

Fluorophore density: Given a configuration of objects \mathbf{x} , the unknown fluorophore density can be defined as follows:

$$R_{\mathbf{x}}(x, y, z) = \sum_{j=1}^{N_{\mathcal{O}}} k_j 1_{\mathcal{O}(\rho_j, \omega_j)}(x, y, z) \quad (3)$$

where $k_j \in \mathcal{K} = [k_{min}, k_{max}]$ $j \in \{1, \dots, N_{\mathcal{O}}\}$ are the objects intensities which have also to be estimated².

3.2. Optimisation Algorithm

The Marked Point Process approach [8, 9] allows to estimate a configuration of objects whose number, location and shape are unknown. The principle consists in the simulation of a Gibbs process defined by the density (against the Poisson process measure):

$$f(\mathbf{x}) = \frac{1}{Z} \exp[-U(\mathbf{x})] \quad (4)$$

where Z is a normalisation factor which can not be computed and U the energy to minimize. In order to simulate this law, a Markov chain which has the stationary distribution f (equation 4) is constructed. The Reversible Jump MCMC embedded in a simulated annealing framework allows to construct a such Markov Chain by using stochastic dynamics. More details on this approach are given in [10]. The energy U is written as the sum of a data term U_d and a prior term U_p which are presented in the latter.

Data term U_d : We denote by b_g a constant that models the background fluorescence produced by parasites light sources in the medium (e.g. autofluorescence, light reflection, fluorescence diffusion in the sample). We can easily estimate b_g from an image region without objects and so, in the following, b_g is supposed to be known. Shot noise have also to be considered in the model. It is inherent to the photon collection process and follows a Poisson distribution.

Let $\mathcal{I}_2^d \in \mathbb{N}$ be the (discrete) image space (i.e. $card(\mathcal{I}_2^d)$ = number of pixels in the data images). For all $i \in \mathcal{I}_2^d$ and for all $l \in \{1, \dots, L\}$, we model the noisy observed discrete signal $S_{il} = S(i, \alpha_l)$ as follows:

$$S_{il} = \mathcal{P}(\beta_{il}) \quad (5)$$

where \mathcal{P} is the Poisson distribution and β_{il} is defined by:

$$\beta_{il} = \int_{A_i} \int_0^\infty (R_{\mathbf{x}}(x, y, z) + b_g) e^{\left(\frac{-z}{d(\alpha_l, \lambda)}\right)} dx dy dz \quad (6)$$

Here, $A_i \subset \mathcal{I}_2$ is the region of \mathcal{I}_2 that corresponds to the pixel $i \in \mathcal{I}_2^d$ and $R_{\mathbf{x}}$ is defined by (3).

From (5) we get, $\forall i \in \mathcal{I}_2^d$ and $\forall l \in \{1, \dots, L\}$, the conditional probability:

$$\mathbb{P}(S_{il} | \mathbf{x}) = \beta_{il}^{S_{il}} \frac{e^{-\beta_{il}}}{S_{il}!} \quad (7)$$

Assuming that observations S_{il} given the configuration \mathbf{x} are pairwise independent $\forall i \in \mathcal{I}_2^d$, $\forall l \in \{1, \dots, L\}$, the joint density function (i.e. the likelihood function of the observations S given a configuration \mathbf{x}) can be written as:

$$\mathbb{P}(S | \mathbf{x}) = \prod_{i \in \mathcal{I}_2^d} \prod_{l=1}^L \mathbb{P}(S_{il} | \mathbf{x}) \quad (8)$$

¹See section 4 for an example where P and M are defined for spheres.

² k_{min} and k_{max} are user defined bounds on the objects intensities.

where $S \in \mathbb{R}^{nL}$ ($n = \text{card}(\mathcal{I}_2^d)$). This assumption can be justified by the fact that for a given configuration \mathbf{x} , the data depend only to the noise, which is pairwise independent $\forall i \in \mathcal{I}_2^d, \forall l \in \{1, \dots, L\}$.

Finally, the data term is defined from the likelihood function (8) by:

$$\begin{aligned} U_d(\mathbf{x}) &= -\log(\mathbb{P}(S|\mathbf{x})) \\ &= \sum_{i \in \mathcal{I}_2^d} \sum_{l=1}^L S_{il} \log\left(\frac{1}{\beta_{il}}\right) + \beta_{il} \end{aligned} \quad (9)$$

Prior term U_p : This term is essential in order to regularize the inverse problem (2). It takes into account some prior information on the solution such as interactions between geometric objects. In this study we focused on vesicle features estimation. Since vesicle should not overlap, we define the following term:

$$U_p^1(\mathbf{x}) = \sum_{u \in \mathbf{x}} \sum_{v \in \mathbf{x}} \Theta(u, v) \quad (10)$$

where $\Theta(u, v)$ is equal to 1 if the objects u and v overlap and 0 otherwise.

We add a second term $U_p^2(\mathbf{x}) = \text{card}(\mathbf{x})$ which penalizes the number of objects in \mathbf{x} . Finally the prior term is given by:

$$U_p(\mathbf{x}) = \gamma_1 U_p^1(\mathbf{x}) + \gamma_2 U_p^2(\mathbf{x}) \quad (11)$$

where γ_1 and γ_2 are the weight assigned to each term.

Finally, we have the global energy $U = U_d + U_p$ which is minimized using the MPP approach briefly presented in section 3.2.

4. EXPERIMENTAL RESULTS

In this section, we present some practical results on synthetic data and real data. Here, we are interested in estimating vesicle features, which are modelled by spherical volumes, $\forall j \in \{1, \dots, N_O\}$:

$$\mathcal{O}(\omega_j) = \mathcal{B}_j = \{(x, y, z) \in \mathbb{R}^3 \text{ s.t. } (12)\} \quad (12)$$

$$(x - c_x)^2 + (y - c_y)^2 + (z - c_z)^2 \leq r^2 \quad (13)$$

where (c_x, c_y, c_z) denotes the center coordinates of the ball \mathcal{B} and r the radius. These parameters belong to the state space $\mathcal{X} = P \times M$ defined by:

$$P = \mathcal{I}_2 \times [0, z_{max}] \quad M = [r_{min}, r_{max}] \quad (14)$$

Here, z_{max} is a boundary of c_z characterized by the deeper penetration depth of MA-TIRFM and, r_{min} and r_{max} are user defined bounds on the radius. A third prior term U_p^3 is defined to penalize objects with $c_z < r$. Note that the method proposed in section 3 can deal with more complex structures than spheres. Indeed, the requirements of the method with respect to the objects' shape are to be able to compute the data term (*i.e.* compute β_{il} (6)) and to determine whether two objects intersect. These requirements can be performed with various shapes even if it means discretizing the β_{il} integral and using a naive method to compute the overlapping (*i.e.* pixel by pixel).

4.1. Using Synthetic Data

The proposed method is evaluated on synthetic noisy data. In order to quantify the robustness of the method with respect to noise, tests under different noise levels have been done. Two different ways are used for varying the noise level in the acquisition simulation. The first one consists in modifying the background fluorescence level (by

varying the b_g constant). In the following, simulated b_g will be given as a percentage of the maximum intensity of the simulated sample. Another way to modify the noise level can be performed by adding a parameter δ as follows:

$$S_{il} = \frac{1}{\delta} \mathcal{P}(\delta \beta_{il}) \quad (15)$$

in order to change the variance of the Poisson distribution, which mimics the photon collection process.

Root mean square errors (RMSE) have been computed for each parameters:

$$RMSE_Y = \sqrt{\frac{1}{N_O} \sum_{i=1}^{N_O} (\hat{Y}_i - Y_i)^2} \quad (16)$$

where \hat{Y} is the estimated parameter and Y the exact value of this parameter.

Figure 2 shows the RMSE for different background fluorescence levels (*i.e.* different values of b_g). We obtain a high accuracy reconstruction with an RMSE less than 10 nm for parameters c_x , c_y and r . A larger RMSE (between 80 and 125 nm, depending on the noise level) is found on the axial position vesicles estimation.

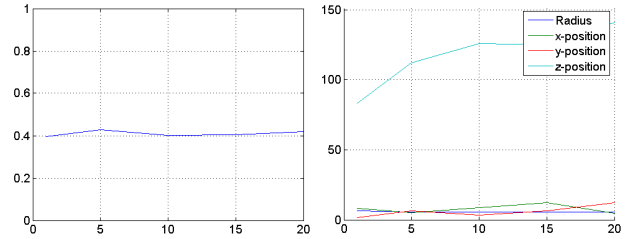


Fig. 2. RMSE with different background fluorescence levels and $\delta = 0.1$. Left : RMSE of objects intensities. Right : RMSE of objects positions and radius.

As we can see on figure 3, the error on the axial position estimation is due to the deepest objects (> 300 nm), objects close to the glass interface are well estimated. Same remarks can be made when we change the Poisson noise (with different values of δ) but due to page limit, results are not presented here.

4.2. Using real Data

The method has also been tested on real data. In order to be able to quantify the quality of the reconstruction, we used a sample of beads of known diameters (170 nm). These beads have been fluorescently labelled and placed at the interface with the glass coverslip in an oil which has the same refractive index as water. The microscope has been developed based on a Nikon Ti-E with 100x/1.490 objective (Nikon). We used an Ixon897 (Andor) for detection and galvanometers mirror (Cambridge Technology) for the control of the illumination angle. The entire system is driven with Labview (National Instruments). Six different incident angles have been used from 63.33° to 79.23° . Figure 4 shows the acquired images for incident angles 63.33° and 79.23° .

Estimated parameters are presented in table 1. Maximal error on the radius is found on the bead 2 with an error of 30 nm (the exact

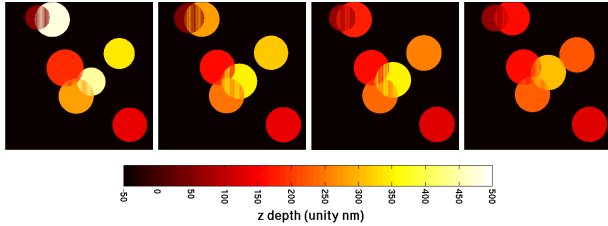


Fig. 3. Reconstructions with different background fluorescence levels and $\delta = 0.1$ (colors represent z positions of objects). From left to right : simulated sample, reconstruction for $b_g = 1\%$, reconstruction for $b_g = 10\%$, reconstruction for $b_g = 20\%$. Data images' size : 50×50 . Reconstructed image size : $50 \times 50 \times 50$. CPU time $\simeq 20$ min on a *hp* Z800 PC with an IntelTM processor (Xeon, 2.40GHz) and a Linux OS. The algorithm is implemented in Matlab.

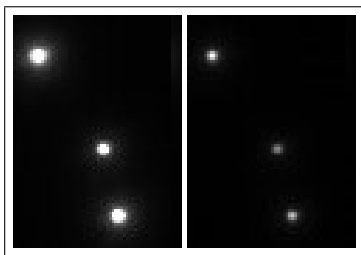


Fig. 4. Real image of beads. Left : $\alpha = 63.33^\circ$. Right : $\alpha = 79.23^\circ$. Data images' size : 60×83 .

radius of the beads is 85 nm). Note that during beads placement at the interface with the glass coverslip, it is not possible to ensure that only one bead is present, there may be a cluster of beads which could explain the estimated radius. Moreover, we can see that found parameters satisfies the property $c_z \simeq r$ meaning that beads are in contact with the glass interface. Although we have not yet studied all microscope uncertainties, which make the reconstruction problem a hard task on real data, these results are promising for feature estimation of predefined shape structures.

Table 1. Estimated parameters. Reconstructed image size : $60 \times 83 \times 50$. CPU time $\simeq 15$ min on the same computer as described in the legend of the figure 3 .

Bead	k	c_x (nm)	c_y (nm)	c_z (nm)	r (nm)
1	0.4	1297.8	1493.1	101.4	101.3
2	0.2	3601.4	4802.3	114.1	114
3	0.3	4118.2	7129.5	91.9	91.6

5. CONCLUSIONS AND FUTURE WORK

We proposed a new model for the reconstruction of three-dimensional structures from a set of 2D images produced by TIRF microscopy. This model takes into account shot noise, background fluorescence and allows multiple objects to be aligned along the axial axis. A Marked Point Process approach is used to estimate objects' parameters with respect to data images. Then we show the robustness of the model with respect to shot noise and background fluorescence.

Future work will focus on microscope calibration in order to improve the reconstruction accuracy on real data. Theoretically, the axial profile of the evanescent wave decreases according to an exponential law (equation (1)). However, it is not the case in practice and experimental calibration of this profile has to be done [5, 11]. We will also investigate the possibility of this model to deal with more complex structures than spheres and the method will be tested in collaboration with biologists for the observation of vesicle involved in cell adhesion mechanism.

6. ACKNOWLEDGMENT

The authors wish to thank E. Van Obberghen-Schilling, A. Radwan-ska and K. Chakrabandhu for providing real samples and interesting discussions regarding biological application of TIRFM.

7. REFERENCES

- [1] GA Truskey, JS Burmeister, E Grapa, and WM Reichert, "Total internal reflection fluorescence microscopy (tirfm). II. topographical mapping of relative cell/substratum separation distances," *Journal of cell science*, vol. 103, no. 2, pp. 491–499, 1992.
- [2] Bence P Ölveczky, N Periasamy, and AS Verkman, "Mapping fluorophore distributions in three dimensions by quantitative multiple angle-total internal reflection fluorescence microscopy.," *Biophysical journal*, vol. 73, no. 5, pp. 2836, 1997.
- [3] Alexander Rohrbach, "Observing secretory granules with a multiangle evanescent wave microscope.," *Biophysical journal*, vol. 78, no. 5, pp. 2641, 2000.
- [4] Dinah Loerke, Walter Stühmer, Martin Oheim, et al., "Quantifying axial secretory-granule motion with variable-angle evanescent-field excitation.," *Journal of neuroscience methods*, vol. 119, no. 1, pp. 65, 2002.
- [5] Qian Yang, Alexander Karpikov, Derek Toomre, and James Duncan, "3D reconstruction of microtubules from multiple-angle total internal reflection fluorescence microscopy using Bayesian framework," *IEEE transactions on Image Processing*, pp. 2248–2259, 2011.
- [6] Liang Liang, Hongying Shen, Yingke Xu, Pietro De Camilli, Derek K Toomre, and James S Duncan, "A Bayesian method for 3D estimation of subcellular particle features in multi-angle tirf microscopy," in *Biomedical Imaging (ISBI), 2012 9th IEEE International Symposium on*. IEEE, 2012, pp. 984–987.
- [7] Daniel Axelrod, Edward H Hellen, and Robert M Fulbright, "Total internal reflection fluorescence," in *Topics in fluorescence spectrometry*, pp. 289–343. Springer, 2002.
- [8] MNM Van Lieshout, "Markov point processes," *Markov point processes and Their Applications*, 2000.
- [9] Xavier Descombes, *Stochastic geometry for image analysis*, Wiley/Iste, x. descombes edition, 2011.
- [10] Peter J. Green, "Reversible jump markov chain monte carlo computation and bayesian model determination," *Biometrika*, vol. 82, pp. 711–732, 1995.
- [11] Alexa L Mattheyses and Daniel Axelrod, "Direct measurement of the evanescent field profile produced by objective-based total internal reflection fluorescence," *Journal of biomedical optics*, vol. 11, no. 1, 2006.